Secondary Structure Mapping of DnaK-Bound Protein Fragments: Chain Helicity and Local Helix Unwinding at the Binding Site†

Zhongjing Chen, Nese Kurt, Senapathy Rajagopalan, and Silvia Cavagnero*

Department of Chemistry, University of Wisconsin, 1101 University Avenue, Madison, Wisconsin 53706

Received June 20, 2006; Revised Manuscript Received August 21, 2006

ABSTRACT: Little is known about polypeptide conformation and folding in the presence of molecular chaperones participating in protein biosynthesis. *In vitro* studies on chaperone−substrate complexes have been mostly carried out with small peptide ligands. However, the technical challenges associated with either competing aggregation or spectroscopically unfavorable size and exchange rates have typically prevented analysis of larger substrates. Here, we report the high-resolution secondary structure of relatively large N-terminal protein fragments bound to the substrate-binding domain of the cotranslationally active chaperone DnaK. The all-α-helical protein apomyoglobin (apoMb), bearing the ubiquitous globin fold, has been chosen as a model substrate. On the basis of NMR secondary chemical shift analysis, we identify, for the first time, weak helical content (similar to that found in the chemically unfolded full-length protein) for the assigned residues of the chaperone-bound chain away from the chaperone binding sites. In contrast, we found that the residues corresponding to the strongest specific binding site for DnaK, examined via a short 13-mer apoMb peptide fragment matching the binding site sequence, display highly reduced helical content in their chaperone-bound form. Given that the free state of the peptide is weakly helical in isolation, we conclude that the substrate residues corresponding to the chaperone binding site undergo helix unwinding upon chaperone binding.

Protein folding is one of the most amazing events in nature. Theoretical and experimental studies have contributed to the understanding of this process for biomolecules able to autonomously fold in buffered solutions (*1*). However, the physical rules governing folding in the context of the more complex biological milieu remain one of the greatest outstanding challenges in modern biology. Molecular chaperones play a seminal role in the cell by assisting folding and protecting nascent polypeptides from misfolding and aggregation (*2*). A better understanding of conformational changes and folding in the presence of chaperones is a key step in learning how proteins reach their native state in nature.

Bacterial Hsp70, better known as DnaK (*3*), is the best-studied chaperone to date. It consists of a highly conserved N-terminal domain (∼44 kDa), containing a nucleotide binding site, and a less conserved C-terminal domain devoted to substrate binding (∼27 kDa). Structural studies on prokaryotic Hsp70 constructs bearing both substrate-binding and ATPase domains have revealed key information about relative interdomain orientation (*4*). Additional high-resolution investigations showed that the substrate-binding domain is divided into a β-sandwich subdomain (ca. residues 393−507) with a peptide-binding cleft and an α-helical latchlike segment (residues 508−638) acting as a lid covering the substrate binding cleft (*5*).

Previous studies on Hsp70−substrate interactions employing entire protein domains or relatively large N-terminal fragments were able to map only biochemical activity and overall physical properties of the bound substrate (*6*−*8*), including the global tertiary structure of the detectable residues (*6*). High-resolution secondary structure information could be obtained for only a few small model peptides known to bind Hsp70. For instance, the study of NRLLLTG (*5*, *9*) and KLIGVLSSLFRPK (*10*) revealed that the chaperone-bound substrate adopts an extended backbone conformation stabilized by backbone hydrogen bonds and nonpolar side chain interactions. These investigations have been extremely informative. However, the substrates mentioned above are either *de novo* peptides with sequences unrelated to those of known proteins (*5*) or peptides derived from proteins of unknown three-dimensional structure (*10*).

To date, there is no high-resolution information about the secondary structure of chaperone-bound peptides derived from proteins of known structure. In addition, virtually nothing is known about the secondary structure of chaperone-bound full-length proteins or large protein fragments. Therefore, it has not yet been possible to evaluate the effect of DnaK on protein conformation.

DnaK recognizes and binds specific primary structural motifs of its substrates. These include four- to five-residue nonpolar sequences, rich in Leu, Ile, Val, Phe, and Tyr, typically flanked by a small number of basic residues (*11*). The binding kinetics is modulated by the different nucleotide binding states of DnaK (*12*). On the other hand, recent evidence suggests that the ATPase domain affects the

† This work was supported by NIH Grant GM068535.

* To whom correspondence should be addressed: Department of Chemistry, University of Wisconsin, 1101 University Ave., Madison, WI 53706. Telephone: (608) 262-5430. Fax: (608) 262-9918. E-mail: cavagnero@chem.wisc.edu.

10.1021/bi0612263 CCC: $33.50
Published on Web 09/19/2006

exchange kinetics but not the conformation of bound substrates (*13*).

DnaK-β (residues 393−507) is the smallest DnaK structural subunit retaining full substrate binding ability. Although the affinity of DnaK-β for small peptide substrates is 15-fold weaker than that of full-length DnaK in the presence of ATP (*14*), and its thermodynamic stability is modulated by the presence of the helical lid (*15*, *16*), it has been shown that DnaK-β retains the ability to bind specific DnaK substrates (*17*). In addition, DnaK-β is able to switch from an open to a closed conformation upon substrate binding, like the full-length chaperone (*12*, *13*). Therefore, DnaK-β is a suitable model system for studies, such as this one, that focus uniquely on the effect of DnaK on the bound substrate conformation. The NMR-friendly tumbling rates of DnaK-β−substrate complexes resulting from their relatively small molecular size facilitate spectroscopic analysis. Consistent with the above, DnaK-β constructs similar to the one employed here were previously used for NMR structural studies in the absence and presence of small peptide ligands (*9*, *14*, *16*). While the prior line of reasoning supports the use of DnaK-β in the present context, it is clear that investigations addressing the role of DnaK in the kinetics and mechanism of protein folding and misfolding are best carried out with the full-length chaperone.

The apomyoglobin (apoMb)[1] sequence is known to have affinity for Hsp70's substrate binding domain, DnaK-β (*6*). ApoMb bears the universally ubiquitous globin fold, and it serves as an archetype for small, single-domain, all-α-helical globular proteins. ApoMb's folding in absence of chaperones is well-characterized (*18*). This protein partially aggregates upon folding from a chemically denatured state (*19*). Full-length apoMb does not significantly bind DnaK-β at equilibrium but appears to bind the chaperone transiently upon folding (*6*). The yield of apoMb refolding increases by ∼36% in the presence of DnaK-β, indicating that this chaperone is involved in the folding/misfolding process. Truncated N-terminal apoMb fragments tend to misfold and form self-associated species in the absence of chaperone (*20*). On the other hand, mixtures of these fragments and DnaK-β (1:1 ratio, each species at ∼100 μM) give rise to a predominantly bound complex (*6*). Hence, the chaperone is able to prevent the misfolding of apoMb fragments. Specific DnaK binding sites along the apoMb sequence have been identified experimentally by cellulose-bound peptide library scanning. The 13-mer peptide HGQDILIRLFKSH, corresponding to residues 24−36 of apoMb's B helix, has the highest binding affinity for both full-length DnaK and DnaK-β (C. Vega *et al.*, submitted for publication). Thus, apoMb is a good model protein for studying the effect of chaperone binding on substrate conformation and folding and misfolding. The structure of apoMb and its fragments used in this investigation are illustrated in Figure 1.

This work provides an initial high-resolution view of the effect of DnaK-β on the secondary structure of apoMb, taken as a model α-helical protein. We report backbone NMR assignments and secondary structure mapping of the chaperone-bound form of two large N-terminal apoMb fragments

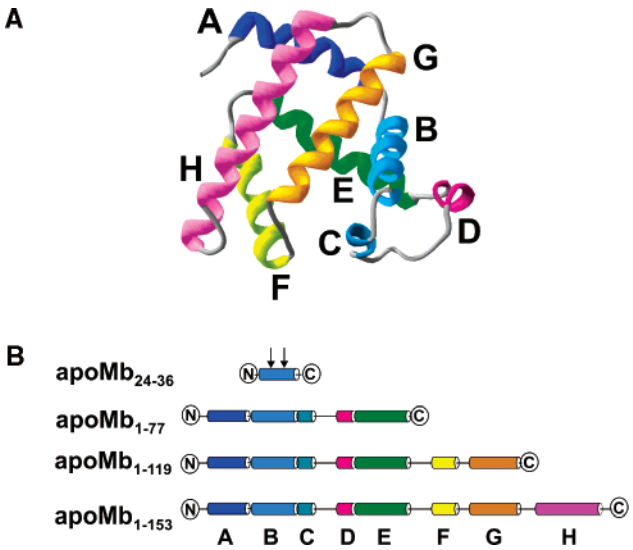

FIGURE 1: (A) Three-dimensional structure of sperm whale myoglobin and (B) cartoon view of the representative N-terminal fragments and chaperone binding site (apoMb$_{24-36}$) investigated in this work. Atomic coordinates for the full-length protein are derived from the PDB file for a high-resolution carbonmonoxy-myoglobin structure (*35*, *36*). Helices are color-coded and labeled A−H (from N- to C-terminus). The image was created with the SwissPdb Viewer software (*37*). Chain lengths and color coding of N-terminal apoMb fragments and apoMb$_{24-36}$ match those for the corresponding helices in the native protein. The vertical arrows in the apoMb$_{24-36}$ cartoon denote the first and last residues of the chaperone binding site core, determined by polypeptide scanning on cellulose support.

(Figure 1), previously known to bind DnaK-β and misfold in the absence of the chaperone (*6*). The specific N-terminal apoMb fragments studied here are representative of the protein chain before it acquires the ability to assume a folded conformation. Here, we also analyze the secondary structure of the 13-mer peptide (HGQDILIRLFKSH) in the absence and presence of DnaK-β. Comparisons with the α-helical content of the same sequence in the full-length native protein lead to the formulation of a specific model for the effect of DnaK on protein conformation.

MATERIALS AND METHODS

Expression and Purification of N-Terminal ApoMb Fragments and DnaK-β Chaperone. Uniformly ^{15}N-labeled and ^{13}C- and ^{15}N-labeled apoMb fragments were overexpressed in *Escherichia coli* in M9 minimal medium containing ^{15}N-labeled NH_4Cl (1.5 g/L) and ^{13}C-labeled glucose (2 g/L) for the doubly labeled species (both purchased from Isotec Inc., Miamisburg, OH). The cell growth and purification procedures for both isotopically labeled apoMb fragments and unlabeled DnaK-β have been described elsewhere (*6*, *20*). Purified DnaK-β was refolded by dropwise dilution into excess 10 mM sodium acetate adjusted to pH 6.0, followed by concentration and overnight dialysis against the same buffer.

ApoMb$_{24-36}$ Peptide Synthesis and Purification. Fmoc-protected uniformly ^{13}C- and ^{15}N-labeled amino acids were purchased from Cambridge Isotope Laboratories (CIL, Andover, MA). ApoMb$_{24-36}$ (HQGDILIRLFKSH-NH_2) was prepared with an automated synthesizer (Applied Biosystems model 432A Synergy) using standard Fmoc (fluorenylmethoxycarbonyl) chemistry. Both natural abundance and

[1] Abbreviations: apoMb, apomyoglobin; HSQC, heteronuclear single-quantum correlation spectroscopy; TOCSY, total correlation spectroscopy; NOESY, nuclear Overhauser enhancement spectroscopy.

^{13}C- and ^{15}N-labeled versions of the peptide were prepared. A methylbenzhydrylamine (MBHA) polystyrene resin functionalized with a 4-hydroxymethylphenoxy (HMP) acid labile linker (Novabiochem, Merck Biosciences AG) was preloaded with an acid labile amine to obtain C-terminal amide-functionalized peptides. A 3-fold excess of activated Fmoc amino acids was used for each coupling. Peptides were cleaved from the resin with a TFA cocktail containing ethanedithiol (2.5%) and thioanisole (5%). Purification was conducted by reverse-phase high-performance liquid chromatography (RP-HPLC) using a Vydac C18 column and a water/acetonitrile (with 0.1% TFA) mobile phase. All peptides were analyzed by matrix-assisted laser desorption ionization time-of-flight (MALDI-TOF) mass spectrometry on a BRUKER REFLEX II instrument. Peptides were stored as lyophilized powders at −20 °C.

NMR Sample Preparation. NMR samples containing apoMb$_{1-77}$ and apoMb$_{1-119}$ were prepared as previously described (*6*). Briefly, acid-unfolded ^{15}N-labeled or ^{13}C- and ^{15}N-labeled apoMb fragments were slowly diluted into a 10 mM acetate buffer at pH 6 containing DnaK-β. The final concentrations of both DnaK-β and apoMb fragments were 100 μM. ApoMb$_{24-36}$ NMR samples were prepared by dissolving the lyophilized powder in 10 mM sodium acetate (pH 6.0) to a total peptide concentration of 1 mM. ApoMb$_{24-36}$ samples containing DnaK-β were prepared by adding the necessary amounts of a ^{13}C- and ^{15}N-labeled version of the above 1 mM apoMb$_{24-36}$ peptide stock solution to DnaK-β-containing solutions in the same buffer to a final peptide concentration of up to 75 μM and a final chaperone concentration of 150 μM. All NMR samples contained 5% (v/v) D_2O and were adjusted to a final pH of 6.0. DnaK-β concentrations were determined by the Bradford Coomassie blue-based protein assay (Pierce, Rockford, IL), against a reference calibration curve obtained by comparing Bradford data to actual DnaK-β concentrations determined by amino acid analysis (University of Iowa Molecular Analysis Facility, Iowa City, IA).

NMR Spectroscopy. NMR data were collected on a Varian INOVA-600 MHz spectrometer. Experiments involving N-terminal apoMb fragments and apoMb$_{24-36}$ were performed at 4 and 30 °C, respectively. A Varian $^1H\{^{13}C,^{15}N\}$ probe with a triple-axis gradient was used, except for the triple-resonance experiments on chaperone-containing samples, which were performed with a Varian triple-resonance $^1H\{^{13}C,^{15}N\}$ cold probe equipped with a *Z*-axis pulsed field gradient.

Backbone resonances of apoMb$_{1-77}$−DnaK-β and apoMb$_{1-119}$−DnaK-β complexes were identified by comparing the assigned ^1H and ^{15}N backbone resonances of the apoMb fragments at pH 2.5 (S. Rajagopalan *et al*., manuscript in preparation) to the titration end-points of experiments on the polypeptide−chaperone complexes (performed with ^{15}N-labeled polypeptides in the presence of unlabeled DnaK-β). Titrations were carried out by collecting series of $^1H-^{15}N$ HSQC data on polypeptide−chaperone complexes at pH 6.0 and progressively lower values, down to pH 2.5. HSQC time-domain data were zero-filled twice and apodized with an unshifted Gaussian in both dimensions. $^{13}C^{\alpha}$ chemical shifts for apoMb$_{1-77}$ and apoMb$_{1-119}$ were obtained by extending the ^1H and ^{15}N assignments to the corresponding $^{13}C^{\alpha}$ resonances via three-dimensional HNCA (*21*). HNCA experiments were carried out at pH 6.0 with 48 (t_1) × 32 (t_2) × 726 (t_3) and 68 (t_1) × 37 (t_2) × 1024 (t_3) complex points for the apoMb$_{1-77}$−DnaK-β and apoMb$_{1-119}$−DnaK-β complexes, respectively. HNCA time-domain data were linearly predicted (32 points) in the ^{15}N dimension and zero-filled twice in all dimensions. Data were then apodized with an unshifted Gaussian in the direct dimension and with a sine-bell square function (90°-shifted for the apoMb$_{1-77}$−DnaK-β complex and 75°-shifted for the apoMb$_{1-119}$-DnaK-β complex) in both the ^{13}C and ^{15}N indirect dimensions.

^1H spin systems for free apoMb$_{24-36}$ were identified by two-dimensional (2D) TOCSY (*22*) (7.5 kHz B_1 field strength, 30 ms spin-lock time) and NOESY (*23*) (300 ms mixing time). $^{13}C^{\alpha}$ and $^{13}C^{\beta}$ assignments for free apoMb$_{24-36}$ were achieved by $^1H-^{13}C$ HSQC and TOCSY, except for $^{13}C^{\alpha}$ of His$_{36}$, which was undetectable. ^{15}N assignments were obtained by complementing TOCSY data with $^1H-^{15}N$ HSQC data. The ^{15}N, $^1H^N$, $^{13}C^{\alpha}$, and $^{13}C^{\beta}$ assignments for DnaK-β-bound apoMb$_{24-36}$ were obtained by a combination of $^1H-^{15}N$ HSQC, $^1H-^{13}C$ HNCACB, $^1H-^{13}C$ HSQC, $^1H-^{13}C$ HCCH-TOCSY, and $^1H-^{13}C$ (H)CCH-TOCSY on a peptide−chaperone sample similar to that employed for the data depicted in Figure 4B. $^1H-^{15}N/^{13}C$ HSQC experiments were performed with the sensitivity-enhanced (SE) HSQC (*24*) pulse sequence. $^1H-^{15}N$ HSQC and $^1H-^{13}C$ HSQC data were acquired with 64 (t_1) × 1024 (t_2) and 200 (t_1) × 1024 (t_2) complex points, respectively. An unshifted Gaussian was applied to the time-domain data, followed by twice zero-filling in both dimensions. Pulsed field gradient 2D $^1H-^{13}C$ HNCACB (*25*), 2D $^1H-^{13}C$ HCCH-TOCSY (*26*), and 2D $^1H-^{13}C$ (H)CCH-TOCSY (*26*) data were acquired for complex sample with spectral widths of 5500 Hz (^1H), and 12 066 Hz (^{13}C); 128 (t_1) × 1024 (t_2) complex points were collected for $^1H-^{13}C$ HNCACB experiments, 200 (t_1) × 512 (t_2) complex points for HCCH-TOCSY experiments, and 212 (t_1) × 512 (t_2) complex points for (H)CCH-TOCSY experiments. Free induction decays were apodized with a 90°-shifted sine-bell square window function and zero-filled twice in both dimensions. Linear prediction (up to twice original data size) was used in the indirect dimension.

The NMRPipe (*27*) and NMRView (*28*) software packages were used for data processing. Proton chemical shifts were referenced relative to external 2,2-dimethyl-2-silapentane-5-sulfonic acid (DSS). ^{15}N and ^{13}C chemical shifts were referenced indirectly (*29*).

Secondary Chemical Shifts. Secondary chemical shifts were calculated by subtracting random coil reference values [Ac-GGXVGG-NH_2 peptides in 1 M urea at pH 5.1 and 25 °C (*30*)] from the experimentally determined chemical shifts of the nuclei of interest. Reference random coil values were corrected for the proximity of proline (*30*).

Circular Dichroism Spectrum of ApoMb$_{24-36}$. Circular dichroism (CD) experiments were performed with an MOS-450 spectropolarimeter from BioLogic (BioLogic Science Instruments, Claix, France). CD data were collected on a 193 μM apoMb$_{24-36}$ sample in 10 mM sodium acetate at pH 6.0 and 30 °C. A 0.1 cm path length quartz cuvette was used (Hellma, Müllheim, Germany). Wavelength scanning was performed in the 193−260 nm spectral region. Data were collected in 1 nm steps, with an acquisition duration of 10 s/nm. Mean residue ellipticities (MRE, in units of degrees

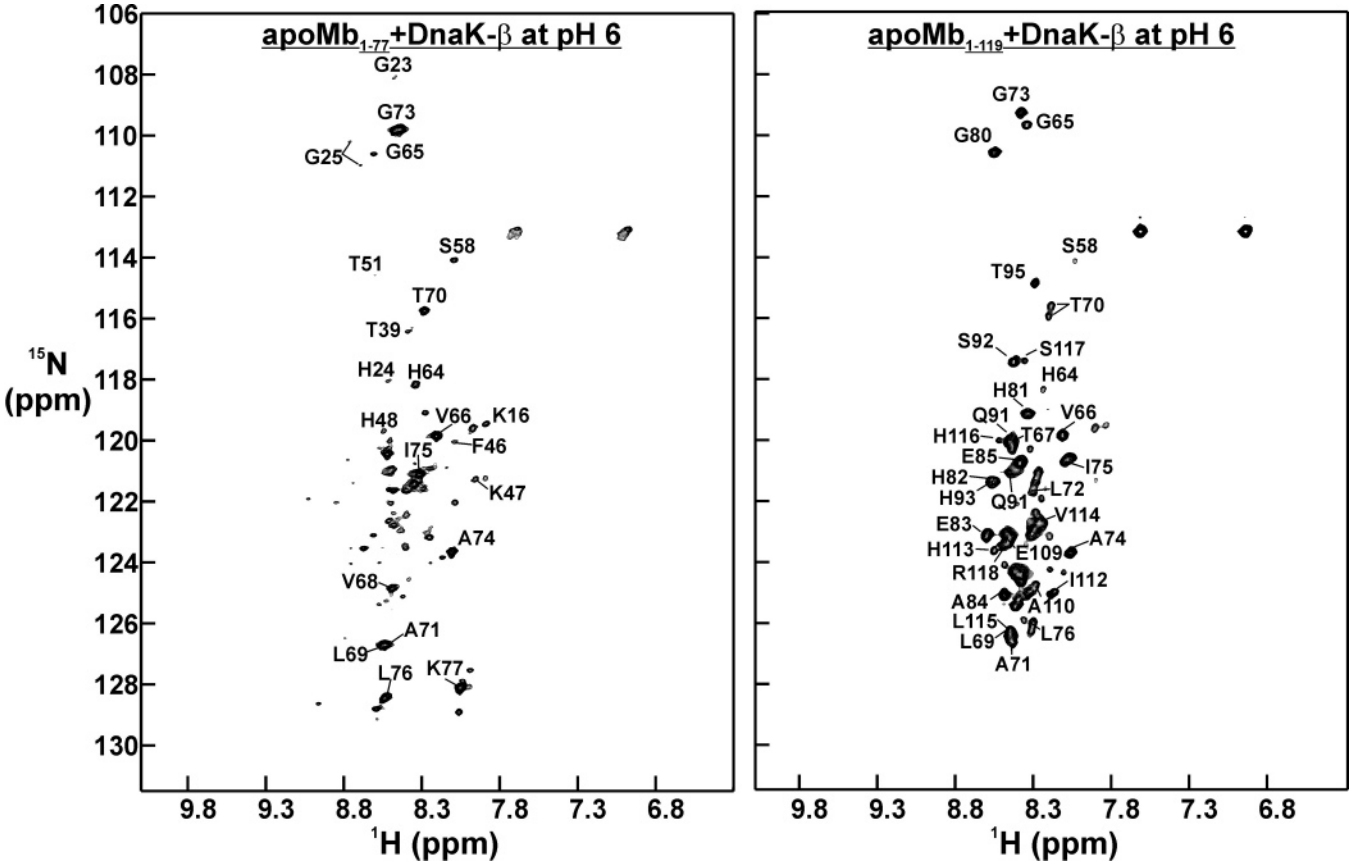

FIGURE 2: $^{1}H-^{15}N$ HSQC spectra of ^{15}N- and ^{13}C-enriched N-terminal apoMb fragments in complex (1:1 molar ratios) with unlabeled DnaK-β. Resonance assignments are labeled on the spectra.

square centimeters per decimole) were calculated according to

$$\mathrm{MRE} = \frac{\theta}{10CN_{\mathrm{A}}l} \quad (1)$$

where θ is the ellipticity in millidegrees, C is the concentration of the protein in moles per liter, N_{A} is the number of amino acids (13 for $apoMb_{24-36}$), and l is the cuvette path length in centimeters.

RESULTS

NMR Assignment of ApoMb N-Terminal Fragments in the Presence of DnaK-β. We previously showed that $apoMb_{1-77}$ and $apoMb_{1-119}$, which are highly prone to misfolding and self-association, are rescued and held in a globally unfolded state when allowed to interact with DnaK-β at 1:1 polypeptide:chaperone ratios (*6*). However, no information about the specific secondary structure assumed by chaperone-bound $apoMb_{1-77}$ and $apoMb_{1-119}$ has been reported so far. To address this important aspect of the chaperone-bound substrate structure, we have carried out NMR backbone resonance assignments of DnaK-β-bound N-terminal apoMb fragments and evaluated NMR secondary chemical shifts of relevant nuclei. Inherent technical difficulties arising from the complex nature of the system required deviations from standard assignment strategies. The synergistic combination of three NMR-based approaches was necessary: (a) triple-resonance experiments followed by complete backbone assignments of the pH-unfolded substrates, (b) pH titrations of the complex from pH 6.0 to the low-pH unfolded state, and (c) HNCA triple-resonance data on the chaperone−substrate complex at pH 6.0 collected on a cold probe (details in Materials and Methods). This strategy led to the first NMR resonance assignments of chaperone-bound large polypeptides. Figure 2 shows the assigned $^{1}H-^{15}N$ HSQC spectra of DnaK-β-bound $apoMb_{1-77}$ and $apoMb_{1-119}$. Complete assignments were not possible due to the relatively high number of missing resonances (especially in the case of $apoMb_{1-119}$) and lack of sequential connectivities. Low signal-to-noise ratios and large tumbling rates were imposed by the small sample concentration and low temperature (4 °C), which were required to minimize competing substrate aggregation. We estimate that exchange broadening does not make a significant contribution to the line shape of the majority of the observed resonances, given that peak intensities are very similar in CPMG-HSQC and reference HSQC spectra (*6*). The presence of some residual chemical exchange on the mid-microsecond time scale, however, cannot be completely ruled out. No assignments could be made for several of the broader resonances and the resonances falling into severely overlapped spectral regions. Interestingly, none of the residues corresponding to the strong chaperone binding site (amino acids 24−32) detected by peptide scanning could be assigned. This is probably due to the efficient relaxation associated with the restricted local motion of the residues directly interacting with the chaperone at 4 °C.

Secondary Structure of ApoMb N-Terminal Fragments in the Presence of the DnaK-β Chaperone. NMR chemical shifts are highly sensitive to electronic environment, which is in turn a good indicator of the degree of tertiary structure. In addition, backbone secondary chemical shifts, i.e., devia-

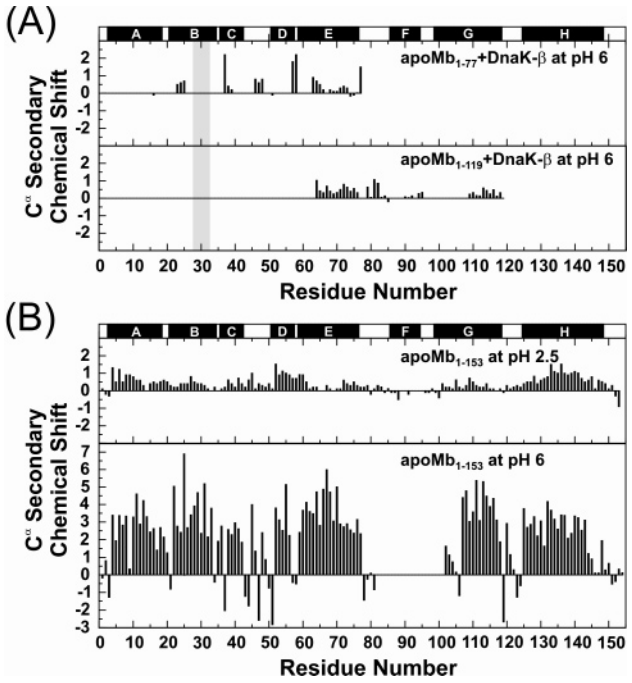

FIGURE 3: (A) C^{α} secondary chemical shifts of $apoMb_{1-77}$ and $apoMb_{1-119}$ N-terminal fragments in the presence of DnaK-β at pH 6 and 4 °C. (B) Known C^{α} secondary chemical shifts of full-length apoMb in its acid-unfolded (pH 2.5 and 25 °C) (*33*) and folded (pH 6.0 and 35 °C) (*32*) states. The gray bar in panel A denotes the chaperone binding site core corresponding to residues 28−32.

tions of the observed shifts from reference random coil values, are also an effective measure of polypeptide secondary structure (*31*). The secondary chemical shifts for the assigned residues of chaperone-bound N-terminal fragments are displayed in the top panel of Figure 3. The bottom panel displays the values for native (*32*) and acid-unfolded (*33*) full-length apoMb, as a reference. As mentioned above, no assignments corresponding to the chaperone binding sites could be made. The assigned residues for the N-terminal chaperone-bound fragments have little α-helical residual secondary structure (Figure 3, top panel). The extent and sequence location of the residual secondary structure are in qualitative agreement with those found in the unfolded full-length protein (Figure 3, bottom panel). Investigations with the peptide corresponding to the specific strong binding site of the apoMb sequence provided additional insights into the local conformational changes associated with chaperone binding.

NMR Assignment of ApoMb$_{24-36}$ in the Absence and Presence of DnaK-β. To monitor the conformation of the residues corresponding to the chaperone binding site, the $apoMb_{24-36}$ peptide, comprising core binding site residues 28−32, has been studied at high resolution. The relatively small size and high solubility of this peptide enable us to obtain a higher-magnitude NMR signal and investigate conformational changes of apoMb upon binding DnaK-β. Chemically synthesized $apoMb_{24-36}$ peptide was selectively labeled with ^{13}C and ^{15}N at G_{25}, L_{29}, L_{31}, F_{33}, and S_{35}. Uniform isotopic labeling was not pursued, given its prohibitive costs. We ensured, however, labeling of leucine at both positions 29 and 31. Leucine is a key residue for DnaK binding (*5*, *11*). Selective isotopic labeling enabled straightforward identification of substrate resonances in the presence

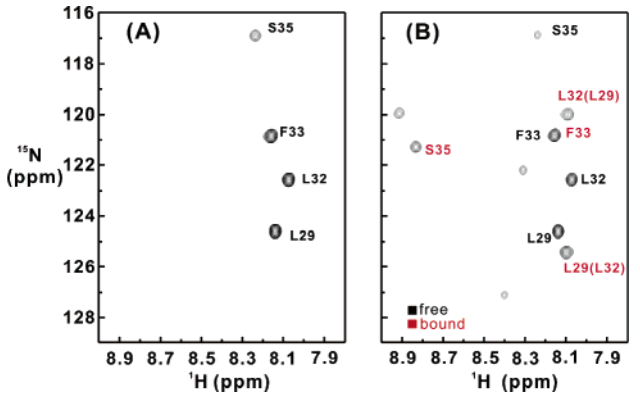

FIGURE 4: 2D $^{1}H-^{15}N$ HSQC spectra of $apoMb_{24-36}$ with specific ^{13}C and ^{15}N labeling in the absence (A) and presence (B) of DnaK-β in 10 mM sodium acetate at pH 6.0. Sample concentrations were as follows: 270 μM $apoMb_{24-36}$ (A) and 75 μM $apoMb_{24-36}$ and 150 μM DnaK-β (B).

of unlabeled chaperone by NMR spectroscopy. Isotropic chemical shifts were exploited as a probe of secondary structure as in the case of the N-terminal fragments. NMR data for $apoMb_{24-36}$ were collected in the absence (Figure 4A) and presence (Figure 4B) of DnaK-β. ^{1}H spin systems for free $apoMb_{24-36}$ were unambiguously assigned by a combination of TOCSY (*22*) and NOESY (*23*) on a 1 mM sample at natural abundance (Figure 5A,B). $^{13}C^{\alpha}$ and $^{13}C^{\beta}$ assignments for free $apoMb_{24-36}$ were achieved on the basis of the assigned ^{1}H chemical shifts (Figure 5C). ^{1}H, ^{15}N, $^{13}C^{\alpha}$, and $^{13}C^{\beta}$ chemical shifts for chaperone-bound $apoMb_{24-36}$ were assigned by analysis of a combination of heteronuclear correlation data collected on the ^{13}C- and ^{15}N-labeled peptide (details in Materials and Methods).

In the presence of a 2-fold excess of DnaK-β, both the free and chaperone-bound forms of $apoMb_{24-36}$ are concurrently observed by NMR. Specifically, the $^{1}H-^{15}N$ HSQC spectra display two distinct sets of resonances due to free and DnaK-β-bound $apoMb_{24-36}$ in slow exchange on the NMR chemical shift time scale (Figure 4B). The ability to directly observe the free and chaperone-bound species undergoing dynamic mutual interconversion provides two key advantages. First, the apparent two-state nature of the transition can be established. Next, a lower limit of ~1 ms can be placed on the bound state lifetime. The dissociation constant for binding of $apoMb_{24-36}$ to DnaK-β, determined by $^{1}H-^{15}N$ HSQC-detected titrations, is 66 ± 14 μM (C. Vega *et al*., submitted for publication). The slow exchange regime coupled to a relatively weak binding affinity is an unusual feature of Hsp70 chaperone binding, and it is entirely consistent with analogous data collected on another peptide (*14*).

Secondary Structure of ApoMb$_{24-36}$ in the Absence and Presence of DnaK-β. Residues 28−32 of apoMb correspond to the highest-affinity binding site for the DnaK chaperone. These residues are included in the $apoMb_{24-36}$ peptide examined here. Figure 6 shows secondary chemical shifts for the assigned resonances of $apoMb_{24-36}$ in the absence and presence of the DnaK-β chaperone (panels B−D), as well as a view of the corresponding shifts for the same residues in the context of the native protein (panel A). Random coil reference values according to Wishart et al. (*30*) were employed here. The consistent pattern of downfield $^{13}C^{\alpha}$ secondary shifts (Figure 6, black bars) indicates that

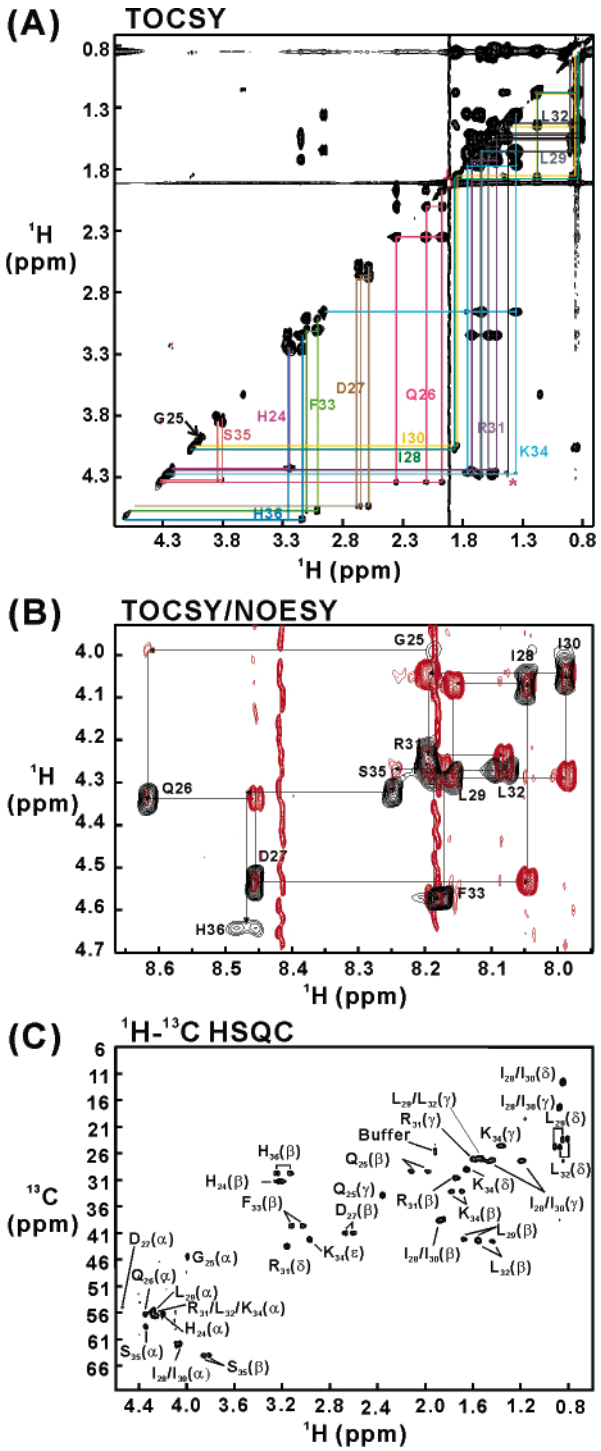

FIGURE 5: 2D NMR spectra of apoMb$_{24-36}$ in the absence of chaperone. (A) Aliphatic region of TOCSY spectrum. The spin system connectivities are shown in color, together with the matching assignments. The asterisk near the blue horizontal line denotes the overlapping connectivities for the H$^{\alpha}$ nuclei of residues L29, L32, and K34. (B) Superposition of H^N−H$^{\alpha}$ regions of TOCSY (black) and NOESY (red) spectra. The lines denote sequential backbone connectivities. (C) Expanded region of the ^{1}H−^{13}C HSQC spectrum of apoMb$_{24-36}$ at natural abundance. The labeled resonances correspond to the assigned ^{1}H chemical shifts from the data in panels A and B. The resonance labeled as Buffer denotes the methyl group of sodium acetate, and it corresponds to the strong diagonal peak at 1.9 ppm in the TOCSY spectrum of panel A. The sample was prepared in 10 mM sodium acetate at pH 6.0.

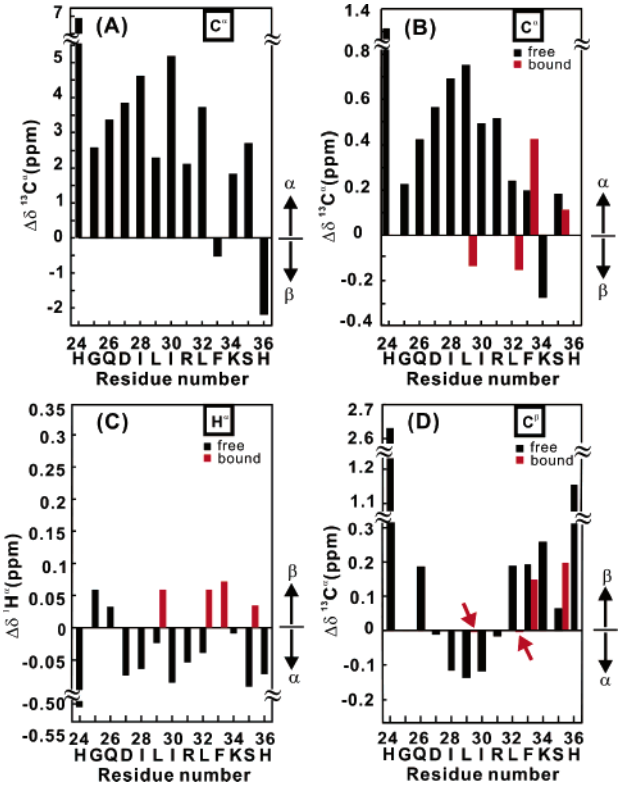

FIGURE 6: Secondary chemical shifts for apoMb$_{24-36}$. (A) C$^{\alpha}$ secondary chemical shifts for amino acids 24−36 of native apoMb (*32*). ^{13}C$^{\alpha}$ (B), ^{1}H$^{\alpha}$ (C), and ^{13}C$^{\beta}$ (D) secondary chemical shifts of apoMb$_{24-36}$ in its free (black) and DnaK-β-bound (red) states. The red arrows in panel D highlight the barely visible secondary chemical shifts of chaperone-bound L29 and L31.

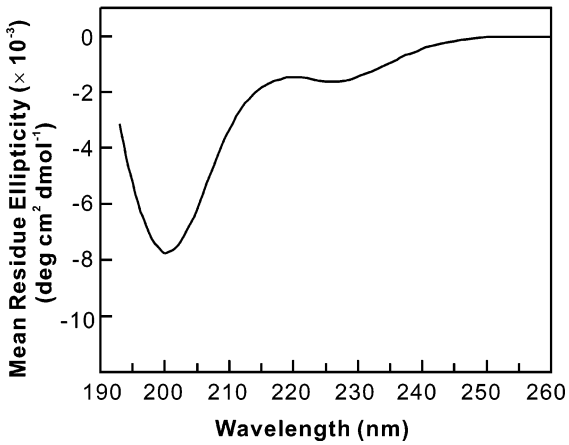

FIGURE 7: Circular dichroism spectrum of 193 μM apoMb$_{24-36}$ in 10 mM sodium acetate at pH 6.0. Data were collected at room temperature.

free apoMb$_{24-36}$ is partially helical. The upfield-shifted H$^{\alpha}$ resonances reflect the presence of some helical population (Figure 6). Far-UV circular dichroism (CD) data for free apoMb$_{24-36}$ (Figure 7) display a doublet between 200 and 230 nm, validating the secondary chemical shift analysis. The combined NMR and CD data indicate that apoMb$_{24-36}$ has an ~15% residual α-helical population in its chaperone-free state.

When DnaK-β binds, significant chemical shift changes are observed for apoMb$_{24-36}$. The ^{13}C$^{\alpha}$ resonances of the key L$_{29}$ and L$_{31}$ residues, both belonging to the high-affinity DnaK binding site (defined by residues 28−32), experience an upfield shift, while H$^{\alpha}$ resonances move downfield. This is consistent with the transition to a nonhelical conformation

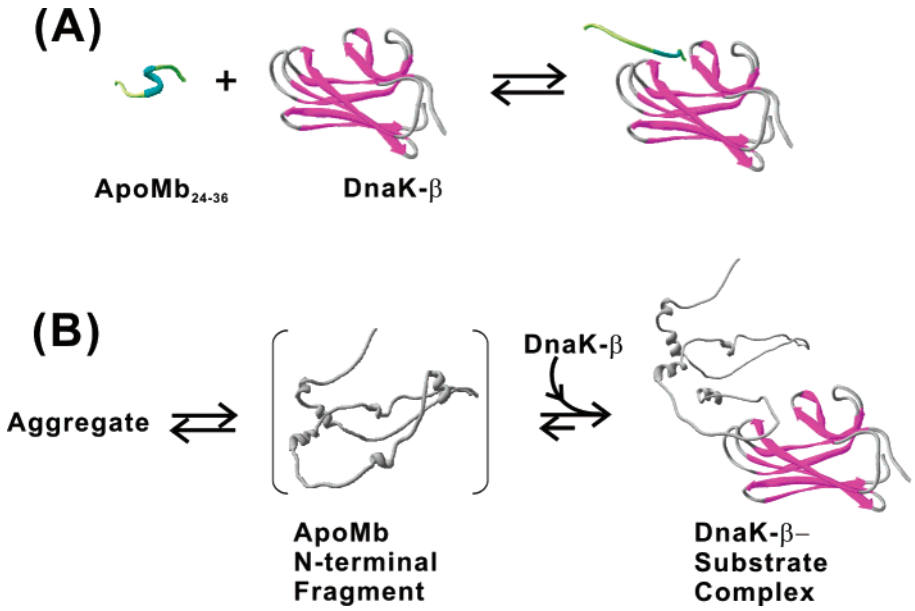

FIGURE 8: (A) Pictorial representation of the effect of DnaK-β on the conformational properties of the apoMb$_{24-36}$ peptide, based on the results of Figure 6. (B) Proposed model for the conformational features of apoMb N-terminal fragments in the presence of the DnaK-β chaperone. The residual helical conformation of the N-terminal fragments is based on the data in Figure 3. The extended conformation at the binding site has been postulated on the basis of the chaperone-bound peptide conformation in panel A. The free monomeric protein fragment in panel B is enclosed in parentheses, as this postulated species cannot be detected under the experimental conditions used in this work. The images were created with the SwissPdb Viewer software (*37*).

for these residues upon chaperone binding. The $^1H^N$ resonance for the bound form of S_{35} experiences a significant downfield shift (Figure 4B), suggesting the formation of stronger backbone hydrogen bonds (*34*) upon complex formation.

DISCUSSION

The NMR resonance assignments and chemical shift analysis of the apoMb$_{1-77}$ and apoMb$_{1-119}$ N-terminal fragments (Figures 2 and 3) provide a first glimpse at the high-resolution secondary structure of a large chaperone-bound polypeptide chain. These fragments encompass the sequence of an all-α-helical protein but are missing the residues corresponding to the C-terminal F−H helices or the H helix. These truncations render the protein fragments incapable of independent native-like folding and make them prone to self-association. DnaK-β is able to prevent this misfolding by keeping the fragments in a globally unfolded state (*6*). We show here that this state, which intrinsically lacks overall tertiary structure, bears some residual helical secondary structure. Interestingly, the extent of helicity is comparable to that observed for the corresponding amino acids in the acid-unfolded state of the full-length protein. This observation, combined with the poor backbone H^N chemical shift dispersion (*6*), suggests that chaperone-bound large protein fragments do not differ much from the unfolded states traditionally employed in classical in vitro refolding experiments, in terms of their general structural features. The presence of the bound chaperone, of course, remains a key distinctive trait (Figure 3).

The analysis of apoMb$_{1-77}$ and apoMb$_{1-119}$ in the presence of DnaK-β described above is based on interpreting the observed C^α chemical shifts as being entirely ascribed to the chaperone-bound form of the substrates. This interpretation is justified by the prior knowledge that a chaperone−substrate dynamic complex is the dominant species in solution under these conditions (*6*). It is worth mentioning, however, that this secondary chemical shift analysis holds true even if small fractions of chaperone-free substrate were to persist in solution.

The residues corresponding to the main chaperone binding site (i.e., amino acids 28−32), which are expected to interact directly with the chaperone, do not display spectroscopically detectable signals. The conformational changes at the binding site, resulting from direct interactions with the chaperone, are of great interest and importance in deciphering chaperone function. The lack of a signal for these residues is likely due to the efficient transverse relaxation resulting from restricted motion and slow molecular tumbling at 4 °C. The resonances for residues 24−32 of apoMb$_{1-77}$ and apoMb$_{1-119}$ cannot be detected by NMR even in the self-associated complex populated in the absence of chaperone (*6*), due to efficient relaxation and/or micro- to millisecond conformational exchange. Chemical exchange does not appear to play a major role, but it cannot be completely ruled out for these residues, both in the absence and in the presence of chaperone (*6*). The highly nonpolar residues 24−32 are expected to be directly involved in the formation of a spectroscopically invisible aggregated core in the absence of the chaperone. Remarkably, in the presence of DnaK-β, the same residues are likely to participate in a direct interaction with the chaperone (C. Vega *et al*., submitted for publication).

The complications in the direct observation of a main chaperone binding site mentioned above were overcome by targeting a decreased molecular size of the complex. This was achieved by analyzing a small peptide substrate corresponding to the major DnaK binding site, apoMb$_{24-36}$. When the chaperone binds, apoMb$_{24-36}$ experiences a significant decrease in its helical content at the residues corresponding to the binding site core. We interpret this event as "local helix unwinding" upon chaperone binding. The HGQDIL-

IRLFKSH sequence is indeed significantly more helical in its free state (Figure 6B−D), in the context of the native protein (Figure 6A), and within the protein unfolded state in aqueous solution (*33*). The two leucines in the binding core turn from a partially α-helical to weakly *β*-strand-like conformation upon chaperone binding (Figure 6B,C). This phenomenon may play a crucial role in the folding of helical proteins in the presence of chaperones.

We previously (*6*) showed that DnaK-*β* is able to prevent the self-association of N-terminal protein fragments of increasing length and increase the yields of correctly folded full-length protein. On the basis of this evidence and the data presented here, we propose the models for the DnaK−substrate interactions shown in Figure 8. DnaK has a pocket for leucine-containing substrates, and it is able to capture misfolding-prone sequences via complex formation. Upon binding DnaK-*β*, apoMb$_{24-36}$ loses its partial helical content (Figure 8A). It is tempting to suggest that a similar transition may take place for the binding of N-terminal fragments to DnaK-*β*, as proposed in Figure 8B. This image also illustrates the residual α-helical character of the N-terminal fragments at regions distant from the binding site. The DnaK−protein fragment complexes shift the equilibrium away from the formation of undesirable aggregates. The complex between the chaperone and large polypeptide substrates is known to be heterogeneous (*6*). Native gel analysis suggested the coexistence of either multiple complexes with a different binding stoichiometry or a unique 1:1 complex with intrinsic conformational heterogeneity (*6*). A combination of both scenarios is also possible. Hence, it is plausible that the chaperone samples more than one substrate binding site. On the other hand, native gel analysis also revealed that a 1:1 overall substrate:chaperone ratio is sufficient for nearly complete complex formation. Therefore, for the sake of simplicity, the general features of the proposed conformational changes upon chaperone binding are illustrated for only an apparent 1:1 binding stoichiometry, in Figure 8B.

Future studies with both the nucleotide-free and ATP/ADP-bound states of full-length DnaK will provide additional evidence that supports this hypothesis.

In summary, we presented, for the first time, residue-specific information about the secondary structure of misfolding-prone large polypeptides in complex with an Hsp70-type chaperone. Our data show evidence for the residual helical content of chaperone-bound N-terminal protein fragments (away from the binding site) and local helical unfolding at the binding site. Therefore, this report provides a glimpse at the remarkable conformational gymnastics associated with the binding of substrates to molecular chaperones.

ACKNOWLEDGMENT

We thank Carolina Vega and Gary Case for technical help with chaperone preparation and peptide synthesis, respectively.

REFERENCES

1. Laurents, D. V., and Baldwin, R. L. (1998) Protein folding: Matching theory and experiment, *Biophys. J. 75*, 428−34.
2. Deuerling, E., and Bukau, B. (2004) Chaperone-assisted folding of newly synthesized proteins in the cytosol, *Crit. Rev. Biochem. Mol. Biol. 39*, 261−77.
3. Mayer, M. P., and Bukau, B. (2005) Hsp70 chaperones: Cellular functions and molecular mechanism, *Cell. Mol. Life Sci. 62*, 670−84.
4. Revington, M., Zhang, Y. B., Yip, G. N. B., Kurochkin, A. V., and Zuiderweg, E. R. P. (2005) NMR investigations of allosteric processes in a two-domain *Thermus thermophilus* Hsp70 molecular chaperone, *J. Mol. Biol. 349*, 163−83.
5. Zhu, X., Zhao, X., Burkholder, W. F., Gragerov, A., Ogata, C. M., Gottesman, M. E., and Hendrickson, W. A. (1996) Structural analysis of substrate binding by the molecular chaperone DnaK, *Science 272*, 1606−14.
6. Kurt, N., Rajagopalan, S., and Cavagnero, S. (2006) Effect of Hsp70 chaperone on the folding and misfolding of polypeptides Modeling an Elongating Protein Chain, *J. Mol. Biol. 355*, 809−20.
7. Langer, T., Lu, C., Echols, H., Flanagan, J., Hayer, M. K., and Hartl, F. U. (1992) Successive action of DnaK, DnaJ and GroEL along the pathway of chaperone-mediated protein folding, *Nature 356*, 683−9.
8. Tanaka, N., Nakao, S., Wadai, H., Ikeda, S., Chatellier, J., and Kunugi, S. (2002) The substrate binding domain of DnaK facilitates slow protein refolding, *Proc. Natl. Acad. Sci. U.S.A. 99*, 15398−403.
9. Stevens, S. Y., Cai, S., Pellecchia, M., and Zuiderweg, E. R. (2003) The solution structure of the bacterial Hsp70 chaperone protein domain DnaK(393−507) in complex with the peptide NRLLLTG, *Protein Sci. 12*, 2588−96.
10. Landry, S. J., Jordan, R., McMacken, R., and Gierasch, L. M. (1992) Different conformations for the same polypeptide bound to chaperones DnaK and GroEL, *Nature 355*, 455−7.
11. Rudiger, S., Germeroth, L., Schneider-Mergener, J., and Bukau, B. (1997) Substrate specificity of the DnaK chaperone determined by screening cellulose-bound peptide libraries, *EMBO J. 16*, 1501−7.
12. Erbse, A., Mayer, M. P., and Bukau, B. (2004) Mechanism of substrate recognition by Hsp70 chaperones, *Biochem. Soc. Trans. 32*, 617−21.
13. Popp, S., Packschies, L., Radzwill, N., Vogel, K. P., Steinhoff, H. J., and Reinstein, J. (2005) Structural Dynamics of the DnaK−Peptide Complex, *J. Mol. Biol. 347*, 1039−52.
14. Pellecchia, M., Montgomery, D. L., Stevens, S. Y., Vander Kooi, C. W., Feng, H. P., Gierasch, L. M., and Zuiderweg, E. R. (2000) Structural insights into substrate binding by the molecular chaperone DnaK, *Nat. Struct. Biol. 7*, 298−303.
15. Moro, F., Fernandez-Saiz, V., and Muga, A. (2004) The lid subdomain of DnaK is required for the stabilization of the substrate-binding site, *J. Biol. Chem. 279*, 19600−6.
16. Swain, J. F., Schulz, E. G., and Gierasch, L. M. (2006) Direct comparison of a stable isolated Hsp70 substrate-binding domain in the empty and substrate-bound states, *J. Biol. Chem. 281*, 1605−11.
17. Gragerov, A., Zeng, L., Zhao, X., Burkholder, W., and Gottesman, M. E. (1994) Specificity of DnaK-peptide binding, *J. Mol. Biol. 235*, 848−54.
18. Nishimura, C., Lietzow, M. A., Dyson, H. J., and Wright, P. E. (2005) Sequence determinants of a protein folding pathway, *J. Mol. Biol. 351*, 383−92.
19. Chow, C., Kurt, N., Murphy, R. M., and Cavagnero, S. (2006) Structural characterization of apomyoglobin self-associated species in aqueous buffer and urea solution, *Biophys. J. 90*, 298−309.
20. Chow, C. C., Chow, C., Raghunathan, V., Huppert, T. J., Kimball, E. B., and Cavagnero, S. (2003) Chain length dependence of apomyoglobin folding: Structural evolution from misfolded sheets to native helices, *Biochemistry 42*, 7090−9.
21. Kay, L. E., Ikura, M., Tschudin, R., and Bax, A. (1990) Three-dimensional triple-resonance NMR spectroscopy of isotopically enriched proteins, *J. Magn. Reson. 89*, 496−514.
22. Cavanagh, J., and Rance, M. (1992) Suppression of Cross-Relaxation Effects in TOCSY Spectra Via a Modified Dipsi-2 Mixing Sequence, *J. Magn. Reson. 96*, 670−8.
23. Lippens, G., Dhalluin, C., and Wieruszeski, J. M. (1995) Use of a Water Flip-Back Pulse in the Homonuclear NOESY Experiment, *J. Biomol. NMR 5*, 327−31.
24. Kay, L. E., Keifer, P., and Saarinen, T. (1992) Pure absorption gradient enhanced heteronuclear single quantum correlation

spectroscopy with improved sensitivity, *J. Am. Chem. Soc. 114*, 10663−5.
25. Muhandiram, D. R., and Kay, L. E. (1994) Gradient-enhanced triple-resonance three-dimensional NMR experiments with improved sensitivity, *J. Magn. Reson., Ser. B 103*, 203−16.
26. Kay, L. E., Xu, G. Y., Singer, A. U., Muhandiram, D. R., and Formankay, J. D. (1993) A Gradient-enhanced HCCH-TOCSY experiment for recording side-chain ^{1}H and ^{13}C correlations in H_2O samples of proteins, *J. Magn. Reson., Ser. B 101*, 333−7.
27. Delaglio, F., Grzesiek, S., Vuister, G. W., Zhu, G., Pfeifer, J., and Bax, A. (1995) NMRPipe: A multidimensional spectral processing system based on unix pipes, *J. Biomol. NMR 6*, 277−93.
28. Johnson, B. A., and Blevins, R. A. (1994) NMRView: A computer-program for the visualization and analysis of NMR Data, *J. Biomol. NMR 4*, 603−14.
29. Wishart, D. S., Bigam, C. G., Yao, J., Abildgaard, F., Dyson, H. J., Oldfield, E., Markley, J. L., and Sykes, B. D. (1995) ^{1}H, ^{13}C and ^{15}N chemical shift referencing in biomolecular NMR, *J. Biomol. NMR 6*, 135−40.
30. Wishart, D., Bigam, C., Holm, A., Hodges, R., and Sykes, B. (1995) ^{1}H, ^{13}C and ^{15}N random coil NMR chemical shifts of the common amino acids. I. Investigations of nearest-neighbor effects, *J. Biomol. NMR 5*, 67−81.
31. Wishart, D. S., Sykes, B. D., and Richards, F. M. (1991) Relationship between nuclear magnetic resonance chemical shift and protein secondary structure, *J. Mol. Biol. 222*, 311−33.
32. Eliezer, D., and Wright, P. E. (1996) Is apomyoglobin a molten globule? Structural characterization by NMR, *J. Mol. Biol. 263*, 531−8.
33. Eliezer, D., Yao, J., Dyson, H. J., and Wright, P. E. (1998) Structural and dynamic characterization of partially folded states of apomyoglobin and implications for protein folding, *Nat. Struct. Biol. 5*, 148−55.
34. Wagner, G., Pardi, A., and Wuthrich, K. (1983) Hydrogen-bond length and H-1-NMR chemical-shifts in proteins, *J. Am. Chem. Soc. 105*, 5948−9.
35. Kuriyan, J., Wilz, S., Karplus, M., and Petsko, G. A. (1986) X-ray structure and refinement of carbon-monoxy (Fe II)-myoglobin at 1.5 Å resolution, *J. Mol. Biol. 192*, 133−54.
36. Berman, H. M., Westbrook, J., Feng, Z., Gilliland, G., Bhat, T. N., Weissig, H., Shindyalov, I. N., and Bourne, P. E. (2000) The Protein Data Bank, *Nucleic Acids Res. 28*, 235−42.
37. Guex, N., and Peitsch, M. C. (1997) SWISS-MODEL and the Swiss-PdbViewer: An environment for comparative protein modeling, *Electrophoresis 18*, 2714−23.

BI0612263